PHYSICAL REVIEW B **85**, 094413 (2012)

Antiferromagnetism in Cr_3Al and relation to semiconducting behavior

Z. Boekelheide,[1,2,*] T. Saerbeck,[3,4] Anton P. J. Stampfl,[3,5] R. A. Robinson,[3] D. A. Stewart,[6] and F. Hellman[1,2]
[1]*Department of Physics, University of California, Berkeley, Berkeley, California 94720, USA*
[2]*Materials Sciences Division, Lawrence Berkeley National Laboratory, Berkeley, California 94720, USA*
[3]*Bragg Institute, Australian Nuclear Science and Technology Organisation, Lucas Heights, New South Wales 2234, Australia*
[4]*School of Physics, University of Western Australia, 35 Stirling Highway, Crawley, Western Australia 6009, Australia*
[5]*School of Chemistry, The University of Sydney, New South Wales 2006, Australia*
[6]*Cornell Nanoscale Facility, Cornell University, Ithaca, New York 14853 USA*
(Received 27 October 2011; revised manuscript received 20 January 2012; published 9 March 2012)

Antiferromagnetism and chemical ordering have both been previously suggested as causes of the observed semiconductorlike behavior in Cr_3Al. Two films of $Cr_3Al(001)/MgO(001)$ were grown under different conditions to achieve different types of chemical ordering and electronic properties: one X-phase structure (semiconducting) and one $C11_b$ structure (metallic). The films were investigated by x-ray and neutron diffraction. Both films show commensurate antiferromagnetic order, with a high Néel temperature greater than 578 K, showing that the antiferromagnetism in Cr_3Al is quite robust. Density-functional theory calculations were performed and it was shown that the well-known antiferromagnetic pseudogap in the density of states occurs for all types of chemical ordering considered. The conclusion of these studies is that the antiferromagnetism causes a pseudogap in the density of states, which is a *necessary* condition for the semiconductorlike transport behavior; however, that antiferromagnetism is seen in both metallic and semiconducting Cr_3Al samples shows that antiferromagnetism is not a *sufficient* condition for semiconducting behavior. Chemical ordering is equally important.

DOI: 10.1103/PhysRevB.85.094413 PACS number(s): 75.50.Ee, 71.20.Lp, 71.23.−k, 75.25.−j

I. INTRODUCTION

The material $Cr_{1-x}Al_x$ exhibits previously unexplained semiconductorlike electronic behavior around the stoichiometry Cr_3Al. Our recent photoemission study showed a narrow gap or pseudogap at E_F in a $Cr_{0.80}Al_{0.20}$ thin film.[1] A high resistivity, up to 3600 $\mu\Omega$ cm, and a large negative Hall constant both peak at $x = 0.25$.[2,3] In addition, the electronic contribution to the specific heat shows a minimum at $x = 0.25$.[4]

The magnetism in $Cr_{1-x}Al_x$ shows anomalous behavior in the same range of x. Antiferromagnetism in Cr occurs in a spin-density wave (SDW) incommensurate with the lattice. With the addition of 3–50 at. % Al, the SDW becomes commensurate with the bcc lattice, like a simple antiferromagnet, shown in Fig. 1(a).[5,6] The Néel temperature T_N and the magnetic moment on the Cr atom increase significantly with the addition of Al, peaking at values above 900 K and $1\mu_B$ around $x = 0.25$.[6–8] The large moment and high Néel temperature are thought to be due to increased localization of the d electrons in $Cr_{1-x}Al_x$ compared to Cr.[9]

These signatures, occurring near $x = 0.25$, point toward a stoichiometric Cr_3Al compound causing the anomalous behavior. Such a compound has been suggested by transmission electron microscopy (TEM), which showed nanometer-size domains of a chemically ordered, rhombohedrally distorted structure separated by antiphase boundaries.[10] The proposed Cr-Al phase diagram puts the phase boundary for this Cr_3Al phase, called the X phase, at 400 °C, above which is a two-phase region of $C11_b$ $Cr_2Al + Cr$.[11] The low-temperature phase boundary explains why the X-phase ordering has been observed only over the short to medium range, as atomic mobility at 400 °C is low. In addition, such a low-temperature phase boundary suggests that the structure of a given sample is likely strongly dependent on preparation conditions. A mechanism for how chemical ordering could lead to the observed semiconductorlike behavior is currently being explored.[12]

The electronic and magnetic properties of Cr_3Al may therefore be expected to depend on the particular chemical ordering seen in a given sample, which in turn likely depends on the preparation conditions. While the electrical resistivity,[2,3] Néel temperature (from susceptibility),[6] and magnetic moment[7] have each been measured for bulk $Cr_{1-x}Al_x$ alloys, these measurements were performed by different researchers on different samples, which may very well have had different properties. In fact, the authors reporting magnetic susceptibility results noted a difference between heating and cooling measurements, suggesting that sample annealing occurred during the measurement, which affected the properties.[6] In the first part of this paper we present neutron-diffraction results on structurally and electrically well-characterized Cr_3Al samples with two different structures in a comprehensive study of the magnetism in Cr_3Al.

The antiferromagnetism itself has also been suggested as a cause for the semiconductorlike behavior. In Cr, the antiferromagnetism splits the d band into two d subbands, one below and one above the Fermi energy E_F. This results in the well-known pseudogap at E_F, with a decreased density of states (DOS) in antiferromagnetic compared to paramagnetic Cr. However, enough sp-like states remain at E_F for Cr to remain a metal.[8] It has been suggested that with the addition of Al, the d subbands are shifted further apart, further decreasing the DOS and leading to the observed transport behavior.[2] However, this model is incomplete because it does not treat the sp states that are primarily responsible for electrical conduction in Cr. In the second part of this paper we use density-functional theory (DFT) calculations to explore how the pseudogap in the DOS is affected by magnetism.

II. EXPERIMENTAL METHODS

The Cr_3Al films were grown epitaxially on MgO(001) substrates by codeposition of Cr from an electron-beam source

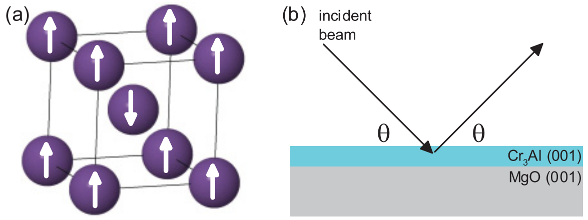

FIG. 1. (Color online) (a) Commensurate spin-density wave (simple antiferromagnetism) on the bcc lattice. (b) Experimental setup for x-ray and neutron-diffraction experiments.

and Al from an effusion cell at a combined growth rate of 0.5 Å/s and a base pressure of 7×10^{-9} Torr. Films of Cr(001) are known to grow epitaxially on MgO(001).[13] The MgO lattice constant is 4.211 Å, or about $\sqrt{2}$ larger than that of Cr. Thus the Cr lattice grows 45° rotated compared to the substrate (Cr[110] || MgO[010]). For pure Cr, the lattice mismatch for this epitaxial relation is 3.9%, while the addition of Al increases the lattice constant and decreases the mismatch to approximately 1% at the Cr_3Al stoichiometry. Epitaxy was verified *in situ* by reflection high-energy electron diffraction, which showed a streaky pattern.

Two films of Cr_3Al were used for the neutron-diffraction study: one 0.95-μm Cr_3Al sample grown at 300 °C and one 1.00-μm Cr_3Al sample grown at 600 °C. The large thickness was chosen to increase the neutron-diffraction intensity. These films are not "thin films" in that their behavior is not significantly affected by confinement effects. However, their structure is certainly affected by the vapor deposition, "thin film" growth technique used to grow them.

X-ray diffraction (XRD) was used to structurally characterize the samples. All Cr-Al diffraction peaks discussed here are indexed in the cubic zone based on a two-atom basis (bcc), as is customary for Cr and its alloys [Fig. 1(a)]. X-ray diffraction measurements were performed using a Panalytical XPert MRD Pro four-circle diffractometer with Cu $K\alpha 1$ radiation. Epitaxy was verified *ex situ* by XRD, which showed fourfold symmetry of the $\{011\}$ peaks in an azimuthal scan at 45° from normal. In addition, only the bcc (001) orientation is seen in XRD θ-2θ scans, shown in Figs. 2(a) and 3(a).

Resistivity of the films was measured as a function of temperature with a van der Pauw technique,[14] with four leads connected to the four corners of the square film samples. High-angle neutron diffraction was performed using the triple-axis spectrometer TAIPAN at Australian Nuclear Science and Technology Organisation,[15] set up to detect elastic diffraction of $\lambda = 2.35$ Å neutrons. A vertically focused pyrolitic graphite monochromator and analyzer were used, with the collimation $48'/40'/40'$/open. Structural and magnetic diffraction peaks were measured between 60 and 639 K in a closed-cycle cryofurnace. The alignment was confirmed at each temperature, using the Cr-Al (002) and (011) (structural) diffraction peaks.

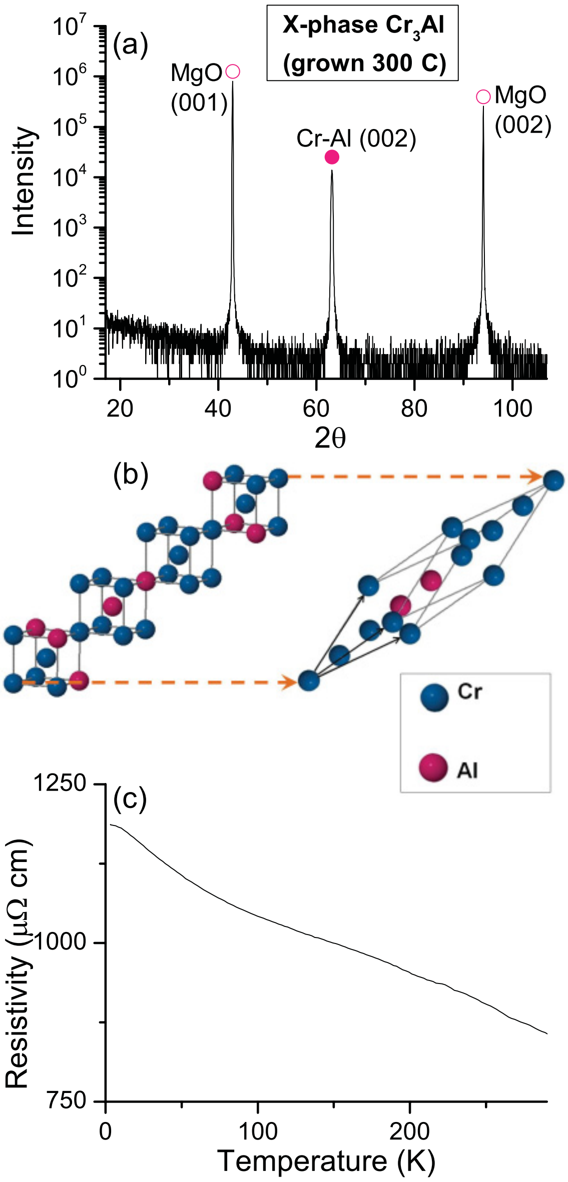

FIG. 2. (Color online) Characterization of the X-phase Cr_3Al 0.95-μm film used for neutron diffraction, deposited at 300 °C. (a) The θ-2θ XRD scan. Solid circles indicate diffraction peaks from the sample, while open circles indicate diffraction peaks from the substrate. An azimuthal ϕ scan (not shown) showed fourfold symmetry, indicating epitaxy. (b) The X-phase Cr_3Al superstructure. Left: rhombohedral structure showing surrounding bcc environment. Right: rhomboid primitive cell. Black arrows are primitive lattice vectors. (c) Resistivity measured by the van der Pauw technique.

III. EXPERIMENTAL RESULTS

X-ray diffraction shows the structural ordering in each sample. The film grown at 300 °C displays a single Cr-Al (002) peak in XRD due to the bcc structure [Fig. 2(a)]. This may be suggestive of a bcc solid solution; however, other factors indicate that this sample most likely has short- to medium-range X-phase chemical ordering of the atoms on the bcc sites. The X phase has a rhombohedral unit cell, shown in Fig. 2(b). The primitive reciprocal lattice vectors are $\frac{1}{4}(\bar{1}\bar{1}3)$, $\frac{1}{4}(\bar{1}3\bar{1})$, and $\frac{1}{4}(3\bar{1}\bar{1})$, thus there are no peaks expected in the (001) out-of-plane XRD scan. Because of the short- to medium-range nature of the ordering, the X phase has never before been observed by even powder XRD, only by diffuse spots in the TEM diffraction pattern. In bulk samples, the

X phase was found to encompass the entire volume of bcc crystallites, but occurred in small (1–3)-nm domains separated by antiphase boundaries.[10] Transmission electron microscopy determination of the X phase in our film samples was not possible due to the small aperture required, leading to an expected intensity of the X-phase peaks below the level of the noise.

This sample has properties that clearly distinguish it from the sample grown at 600 °C, which will be discussed below. It is thought to be an X phase rather than a bcc solid solution for a number of reasons. First, the X phase is the equilibrium structure for Cr$_3$Al below 400 °C on the proposed phase diagram.[11] Second, the X phase is found to be the structure with the lowest ground-state energy from DFT calculations, shown in Sec. V and Ref. 12, and therefore most likely to occur in nature. Third, the semiconductorlike transport behavior is indicative of the X phase, as discussed below. We call this the X-phase Cr$_3$Al sample.

The film grown at 600 °C, in contrast, displays the bcc Cr-Al (002) peak as well as $(00\frac{2}{3})$, $(00\frac{4}{3})$, and $(00\frac{8}{3})$ superlattice peaks indicating $C11_b$ ordering [Fig. 3(a)]. The $C11_b$ unit cell contains three bcc unit cells, with layers of Cr and Al atoms (Cr-Cr-Al-Cr-Cr-Al. . .). This structure is the equilibrium phase for the Cr$_2$Al stoichiometry, with the single phase region for this phase extending across the range $x \sim 0.28$–0.35. For the Cr$_3$Al stoichiometry, a two-phase Cr$_2$Al + Cr region is shown in the phase diagram above 400 °C.[11] However, no evidence of phase separation, which would lead to a splitting of the Cr-Al (002) bcc peak, is seen in the XRD data for our film. Instead, in this film, we observe an off-stoichiometry, single-phase $C11_b$ Cr$_3$Al compound, or $\mathrm{Cr_2(Al_{1-\delta}Cr_\delta)}$ with $\delta = 0.25$, with Cr presumably substituting onto the Al sites. This structure is shown in Fig. 3(b). This is supported by the decrease in tetragonal distortion in this film compared to $C11_b$ Cr$_2$Al (in our film, $a = 2.95$ Å, $c = 8.75$ Å, or 1% distortion; in bulk Cr$_2$Al, $a = 3.001$ Å, $c = 8.637$ Å, or 4% distortion[6]). We call this the $C11_b$ Cr$_3$Al sample. Although single-phase $C11_b$ Cr$_3$Al does not appear on the equilibrium phase diagram, nonequilibrium structures are often caused by thin-film growth methods due to the kinetics of phase nucleation, surface energy effects during growth, or epitaxy.

The electronic behavior of the X-phase and $C11_b$ films is significantly different. Resistivity vs temperature curves are shown in Figs. 2(c) and 3(c). The X-phase film shows semiconductorlike behavior, with a high residual resistivity at approximately 1200 $\mu\Omega$ cm, and a strongly negative $d\rho/dT$. This is further indication that this sample is indeed an X phase rather than a bcc solid solution, as the X phase has been shown to have a semimetallic band structure (see Sec. V and Ref. 12). The $C11_b$ film, in contrast, has a lower residual resistivity at approximately 450 $\mu\Omega$ cm and a positive $d\rho/dT$ like a conventional metal. Some X-phase Cr$_3$Al samples have been shown to have higher resistivity than the one shown here, up to 2400 $\mu\Omega$ cm in thin films[12] and 3600 $\mu\Omega$ cm in bulk.[2,3] The lower resistivity seen in the 1-μm sample may be due to a slight concentration gradient through the sample from deposition rates drifting during the long vapor deposition process required to reach such a large thickness or due to geometrical errors stemming from use of the van der Pauw technique on a square sample rather than a lithographically patterned sample.

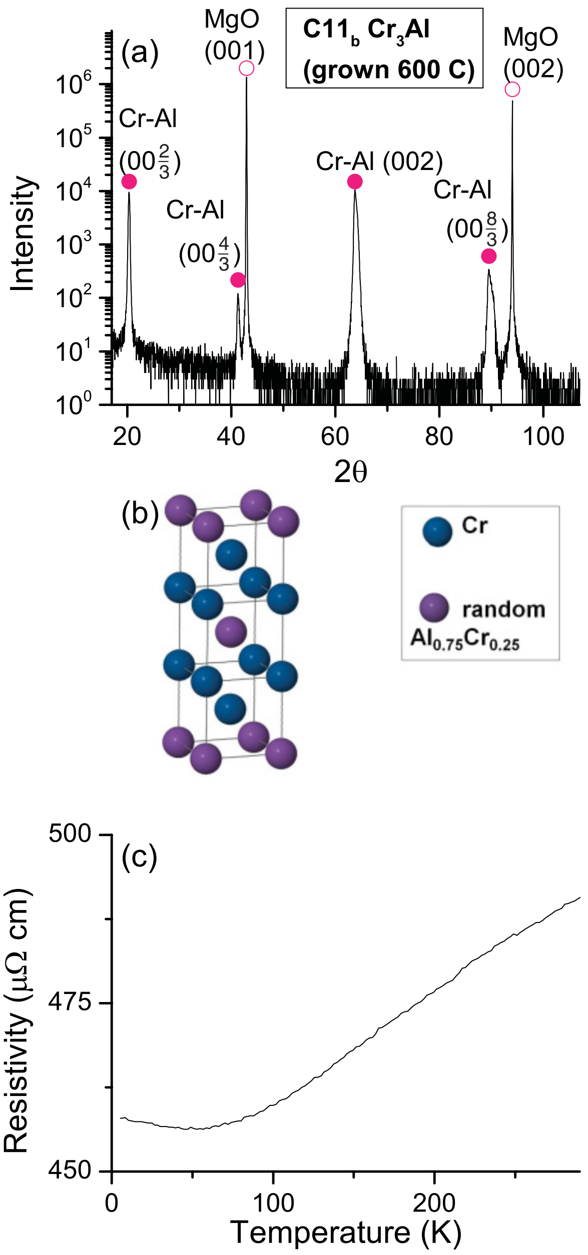

FIG. 3. (Color online) Characterization of the $C11_b$ Cr$_3$Al 1-μm film used for neutron diffraction, deposited at 600 °C. (a) The θ-2θ XRD scan. Solid circles indicate diffraction peaks from the sample, while open circles indicate diffraction peaks from the substrate. An azimuthal ϕ scan (not shown) showed fourfold symmetry, indicating epitaxy. (b) The $C11_b$ Cr$_3$Al superstructure. (c) Resistivity measured by the van der Pauw technique.

Figure 4 shows the magnetic (001) and structural (002) neutron-diffraction peaks as a function of temperature. The structural (002) peak matches the lattice constants determined by XRD. An Al (022) peak is also observed due to the Al sample holder used in the neutron experiments. Note that Al (022) is not seen in XRD [Figs. 2(a) and 3(a)], confirming that the Al (022) peak does not originate from the sample.

The (001) peak is symmetry forbidden for the bcc crystal structure and is not seen in XRD. Thus its existence in neutron diffraction is confirmation of antiferromagnetic ordering in

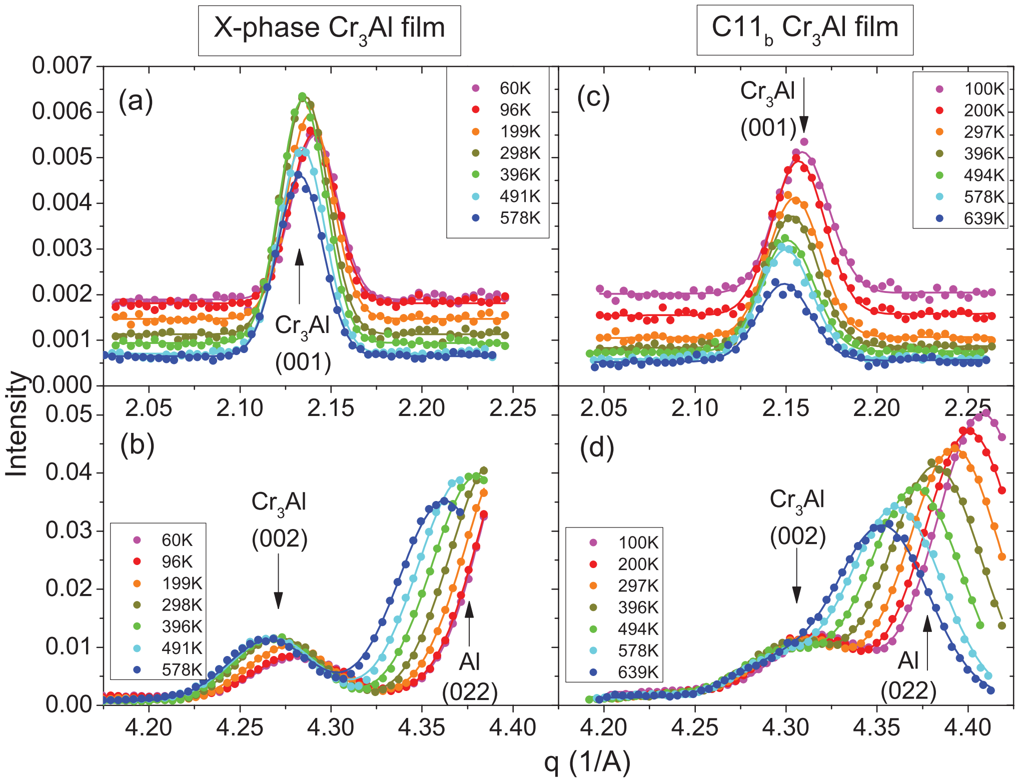

FIG. 4. (Color online) (a) and (c) Antiferromagnetic (001) and (b) and (d) structural (002) neutron-diffraction intensities observed in the (a) and (b) X-phase and (c) and (d) $C11_b$ Cr_3Al films. The lines are Gaussian fits to the data to determine the integrated peak intensity.

both samples, specifically a commensurate SDW or simple antiferromagnetism as shown in Fig. 1(a). In contrast, the incommensurate SDW seen in pure Cr would result in multiple satellite peaks around the (001) peak,[8,16] which are not seen here. It should be noted that the (001) peak is not a result of $\lambda/2$ contamination of the neutron beam, which has been attenuated by a graphite filter to a level of 0.2% of the neutron intensity, negligible compared to our measured (001) peaks, which are about 50% of the (002) intensity.

The experimentally determined magnetic moment on the Cr atoms was found by a comparison of experimental magnetic and structural intensities with calculated intensities obtained from neutron structure factor calculations,[17]

$$S_{\mathrm{Cr}}^{\mathrm{expt}} = \sqrt{\frac{I_{\mathrm{expt}}^{(001)} / I_{\mathrm{expt}}^{(002)}}{I_{\mathrm{calc}}^{(001)} / I_{\mathrm{calc}}^{(002)}}} \times S_{\mathrm{Cr}}^{\mathrm{theor}}, \tag{1}$$

in which $S_{\mathrm{Cr}}^{\mathrm{theor}}$ is an initially assumed theoretical moment of $1\mu_B$. Long-range chemical ordering was not included in the structure factor calculations. Experimental intensities were obtained by integration of Gaussian functions fitted to the beam monitor count and instrumental background corrected data. Calculations of expected intensities were performed including corrections for a temperature-dependent Debye-Waller factor,[18] a Lorentz factor, and a geometrical factor correcting for the experimental diffraction geometry and neutron absorption.[19] The magnetic moment on the Al atoms was assumed to be negligible.[20]

Because magnetic scattering only occurs for the component of the moment that is normal to the scattering vector, an assumption must be made about the direction of the moment in the samples. In pure Cr, the moment aligns along the cube axes. We assume an isotropic distribution of domains with moments along the three cube axes, so that two-thirds of the domains contribute to diffraction of the neutron beam. Alternatively, $C11_b$ Cr_2Al has been shown to have the Cr moment direction along the bcc ⟨111⟩ axis, which would result in an equivalent factor in the moment calculation. Using either of these assumptions, the resulting Cr moment as a function of temperature is shown in Fig. 5.

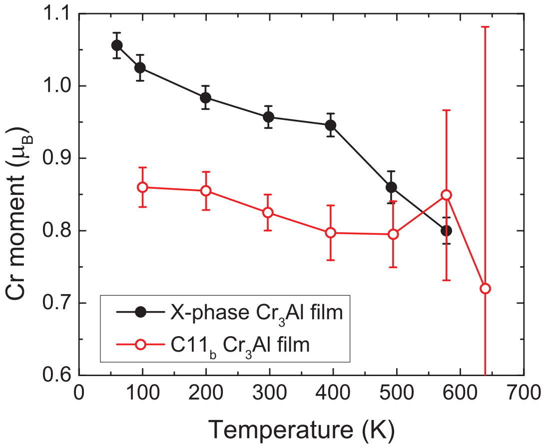

FIG. 5. (Color online) Magnetic moment on Cr atom vs temperature from neutron diffraction of the X-phase and $C11_b$ Cr_3Al films.

TABLE I. Experimental magnetic state, moment, and Néel temperature for Cr, Cr_3Al, and Cr_2Al for our films and bulk samples from the literature. The magnetic moment is given for the lowest temperature measured (well below T_N) for each sample. AF denotes antiferromagnetic.

Composition	Sample type	Crystal structure	Magnetic state	Magnetic moment on Cr atom (μ_B)	Néel temperature (K)
Cr	bulk	bcc	incommensurate SDW[a]	0.43[a,b]	311[a]
Cr_3Al	bulk	unknown	simple AF[c]	1.07[c,d]	913[e]
Cr_3Al	300 °C grown film	X phase	simple AF[f]	1.06 ± 0.02[f,g]	>578[f]
Cr_3Al	600 °C grown film	$C11_b$	simple AF[f]	0.86 ± 0.03[f,h]	>639[f]
Cr_2Al	bulk	$C11_b$	simple AF[i]	0.92 ± 0.02[i,j]	598[i]

[a] Reference 8.
[b] The rms moment of incommensurate SDW, measured at 4.2 K.
[c] Reference 7.
[d] The moment of Cr_3Al composition not measured; the value is for the closest composition ($Cr_{0.80}Al_{0.20}$), measured at room temperature.
[e] Reference 6.
[f] This work.
[g] Measured at 60 K.
[h] Measured at 100 K.
[i] Reference 22.
[j] Measured at 4.2 K.

The primary conclusion from this data is that the antiferromagnetism in both Cr_3Al samples is robust, extending to the highest temperatures measured (578 and 639 K in the X-phase and $C11_b$ samples, respectively). The temperature dependence of the moment in both samples is slight, suggesting that the Néel temperature is significantly higher than the temperatures measured. The large error in the high-temperature data points of the $C11_b$ sample is due to the interference of the Al (022) peak in calculating the intensity of the Cr-Al structural (002) peak (see Fig. 4).[20]

Table I tabulates experimental magnetic parameters of Cr and Cr-Al compounds from the literature along with our results. This work measures the magnetic moment value in Cr_3Al. The closest comparison in the literature is a bulk $Cr_{0.80}Al_{0.20}$ sample, which was reported to have a $1.07\mu_B$ moment on the Cr atom.[7] Our X-phase Cr_3Al film compares well, with a moment of $1.06\mu_B \pm 0.02\mu_B$. However, the $C11_b$ film has a significantly lower moment of $0.86\mu_B$.

The $C11_b$ Cr_3Al may be expected to behave more like $C11_b$ Cr_2Al, which is a known metallic antiferromagnet. Bulk Cr_2Al has a lower magnetic moment[22] of $0.92\mu_B$, which is much closer to that of our $C11_b$ Cr_3Al film. However, bulk Cr_2Al also has a lower Néel temperature[22] of 598 K, while our film shows no hint of the Néel transition up to 639 K. This nonequilibrium $C11_b$ Cr_3Al film thus has magnetic behavior between that of bulk Cr_3Al and Cr_3Al.

The conclusion of these experiments is that robust antiferromagnetism occurs in Cr_3Al regardless of the preparation conditions, chemical ordering, and resultant electronic transport properties. However, there is a significant dependence of the moment on these factors.

IV. THEORETICAL METHODS

Density-functional theory calculations were done using the AKAIKKR code, a full-potential DFT Green's function approach based on the Korringa-Kohn-Rostoker multiple-scattering technique.[23–25] The number of irreducible k points used for Brillouin-zone integration was between 3009 and 3276 for the different structures. The scalar relativistic approximation was used and the generalized gradient approximation (GGA) was used to approximate the exchange-correlation energy.[26]

Calculations were done for pure Cr, Cr_2Al in the $C11_b$ structure, and four different possible Cr_3Al structures. The Cr_3Al structures considered were a bcc solid solution of $Cr_{0.75}Al_{0.25}$; the off-stoichiometric $C11_b$ Cr_3Al structure observed experimentally in our 600 °C grown films; the well-known $D0_3$ (binary Heusler) structure; and finally X-phase Cr_3Al, shown in Fig. 2(b). These structures are all discussed in further detail elsewhere.[12] Disorder in the bcc solid solution and $C11_b$ Cr_3Al structures was treated using the coherent potential approximation.[27,28] Both spin-polarized and nonmagnetic density-functional calculations were performed for each structure.

Pure Cr was treated in the basic bcc unit cell, forcing a commensurate SDW (simple antiferromagnetism) rather than the incommensurate SDW seen experimentally. The incommensurate SDW in Cr not only requires a computationally difficult large unit cell but is, as of yet, not found to be the minimum-energy state in current DFT calculations.[29]

V. THEORETICAL RESULTS

The magnetic parameters obtained from the calculations are tabulated in Table II. For all structures, neighboring Cr moments were found to align antiferromagnetically, with negligible moments on the Al atoms. For the X-phase, $C11_b$, and $D0_3$ Cr_3Al structures, there are multiple Cr sites with different moments. In the case of the $C11_b$ and X-phase structures, the net moment in the unit cell is zero, so the material is antiferromagnetic. However, in the $D0_3$ structure, there is a net moment in the unit cell, signifying ferrimagnetism. This is consistent with calculations by other researchers.[30]

The resulting moments from these calculations are all larger than is experimentally seen. The large calculated Cr moment is consistent with calculations in the literature and is due to

TABLE II. Theoretical magnetic state and moment for Cr, Cr_3Al, and Cr_2Al from our calculations.

Stoichiometry	Crystal structure	Magnetic state	Magnetic moment on Cr atoms (μ_B)
Cr	bcc	simple AF[a]	1.05
Cr_3Al	bcc solid solution	simple AF	1.68
Cr_3Al	$C11_b$	commensurate SDW	1.76, 1.74[b]
Cr_3Al	$D0_3$	ferrimagnetic[c]	↑2.16, ↑2.16, ↓1.75
Cr_3Al	X phase	commensurate SDW[d]	1.65, 1.49, 1.36[e]
Cr_2Al	$C11_b$	AF	1.82

[a] Calculation in the bcc unit cell forces simple antiferromagnetism.

[b] Moment of a Cr atom on a Cr site and substituted onto an Al site, respectively.

[c] Also see Ref. 30.

[d] The wavelength of the SDW is the length of the rhombohedral unit cell.

[e] Six Cr atoms in the primitive X-phase unit cell have ↑ and ↓ of each of these three moment values.

overestimation of the moment by the GGA.[29] However, the trend of increased moment in Cr-Al alloys and compounds compared to Cr is consistent with experiment.

The DOS for each structure is shown in Fig. 6, with the results from magnetic and nonmagnetic calculations compared. The DOS of pure Cr shows the well-known phenomenon of an antiferromagnetic pseudogap opening up at E_F due to an effective doubling of the lattice constant. This pseudogap results in a significant decrease in the DOS(E_F) of Cr; however, states still remaining at E_F lead to the well-known metallic behavior of Cr. These conducting states can be seen in the band structure as wide, sp-like bands crossing E_F.[8]

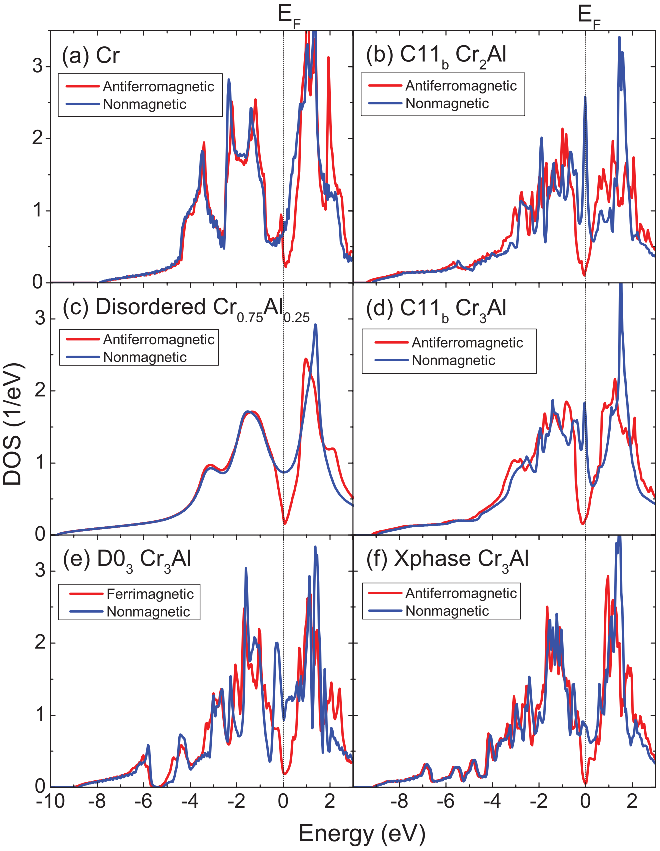

FIG. 6. (Color online) Theoretical density of states of Cr, Cr_2Al, and Cr_3Al with four different types of chemical ordering. The calculations compare magnetic and nonmagnetic cases.

Figure 6 shows the same pseudogap phenomenon for all Cr-Al alloys and compounds considered. In all cases, the DOS(E_F) is significantly decreased by the effect of magnetism. In a mean-field model, the magnetic moment is proportional to the SDW gap and thus may be expected to influence the transport behavior. However, the antiferromagnetic pseudogap alone cannot explain the semiconducting behavior seen experimentally in Cr_3Al. The antiferromagnetic pseudogap and semiconducting gap seem to be separate entities, with the antiferromagnetic pseudogap around 300 meV (Ref. 31) and the semiconducting gap (or pseudogap) estimated between 40 and 95 meV.[1,2,31] This suggests that the magnetism and semiconducting behavior originate from different parts of the band structure.

The calculations showed that the X-phase structure has the lowest total energy, suggesting that it should be the equilibrium structure at low temperatures. The X-phase chemical ordering has also been suggested as one route to explain the semiconducting behavior in Cr_3Al.[12] The band structure of the X phase, shown in Fig. 7(a), is a semimetallic-type band structure with a pseudogap. The nonzero DOS(E_F) is the result of slightly overlapping flat band edges at E_F. The semiconductorlike transport behavior can be explained by the calculated semimetallic band structure, as the flat band edges are more easily affected by localization than wider bands. Figure 7(b) shows the band structure of X-phase Cr_3Al when magnetism is not included in the calculation. Antiferromagnetic X-phase Cr_3Al clearly shows the pseudogap at E_F, while nonmagnetic Cr_3Al has several wider bands crossing E_F, suggesting a metal.

It should be noted that DFT sometimes underestimates band gaps,[32] so an ideal crystal of X-phase Cr_3Al could be fully semiconducting. However, currently available samples are not ideal and are consistent with a semimetallic model (nonzero Sommerfeld coefficient,[4] nonzero photoemission intensity at E_F,[1] and resistivity rising algebraically with decreasing temperature[2,3]). To differentiate between a full band gap or pseudogap requires further work.

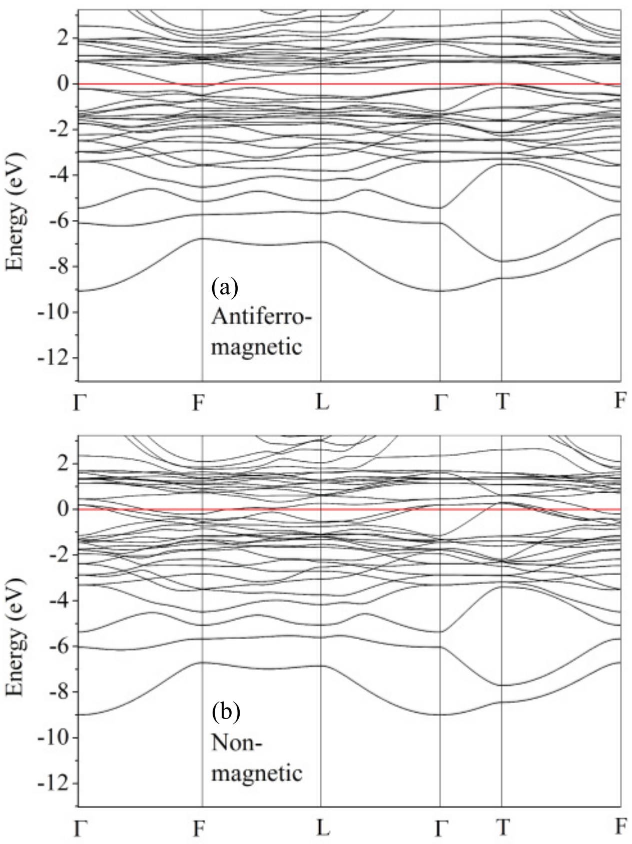

FIG. 7. (Color online) Band structure for Cr_3Al with X-phase ordering for both the antiferromagnetic and nonmagnetic cases.

VI. DISCUSSION

The question of whether magnetism is a cause of the semiconductorlike behavior in Cr_3Al can be answered by testing the logic statement, "If Cr_3Al is magnetic, it is semiconducting," and its inverse, "If Cr_3Al is not magnetic, it is not semiconducting." Our theoretical calculations, presented in Sec. V, suggest that these statements are both true because the low DOS and pseudogap occur only in the antiferromagnetic state. Early calculations of the electronic structure of $Cr_{1-x}Al_x$ did not take into account the antiferromagnetism and thus did not show the split d subbands in the DOS.[33] Those calculations not only showed a high electronic DOS for Cr, in disagreement with specific-heat results, but they showed an increasing DOS with the addition of Al rather than decreasing as was seen from specific heat[4] and as would be expected based on the observed semiconductorlike transport behavior.

Experimentally, two studies have attempted to test these statements by measuring electrical resistivity above and below T_N, drawing different conclusions.[2,34] Because of the high T_N and transport behavior indicative of a narrow gap semiconductor or semimetal, metallic behavior is observed near T_N. In addition, magnetic transitions are expected to influence the resistivity (as seen in Cr); this can be difficult to separate from a semiconductor-to-metal transition.[8] Thus the previous conflicting experimental studies were never resolved.

While experimentally testing the above statements has proven difficult, the converse and contrapositive can be tested: "If Cr_3Al is semiconducting, it is magnetic" and "If Cr_3Al is not semiconducting, it is not magnetic." The experimental work presented here provides a test of these statements. The two films studied, the X-phase and $C11_b$ Cr_3Al films, are semiconducting and metallic, respectively. Both are shown to be antiferromagnetic by neutron diffraction. Thus the statement, "If Cr_3Al is semiconducting, it is magnetic" is true, while the statement, "If Cr_3Al is not semiconducting, it is not magnetic" is false. The conclusion of our tests of these logic statements is that magnetism is a *necessary* condition for semiconducting behavior in Cr_3Al, but it is not *sufficient*. We suggest that the semimetallic gap in X-phase Cr_3Al is a result of both the antiferromagnetism forming a gap in the d-like bands and chemical ordering forming a gap in the sp-like bands.

VII. CONCLUSION

We conclude that both antiferromagnetism and chemical ordering play an important role in the anomalous transport behavior of Cr_3Al. The theoretical results presented here show clearly that for any Cr-Al structure, magnetism is a necessary ingredient for the creation of a pseudogap at E_F. Destruction of magnetism in Cr_3Al would likely result in a return to metallic behavior if it could be achieved. Our neutron-diffraction results show that while manipulation of growth conditions leads to a nonequilibrium structure and either semiconducting or metallic behavior, the antiferromagnetism is quite robust. In this case, the main difference between the two Cr_3Al films, one semiconducting and the other metallic, is the chemical ordering and not the magnetism. This highlights the importance of chemical ordering and structure to the semiconducting behavior in Cr_3Al, which will be explored further in future work.

ACKNOWLEDGMENTS

This work was supported by the US Department of Energy under Contract No. DE-AC02-05CH11231. Calculations were done at the Cornell Nanoscale Facility, part of the National Nanotechnology Infrastructure Network funded by the National Science Foundation.

---

[*] Present address: Material Measurement Laboratory, National Institute of Standards and Technology, Gaithersburg MD 20899; zoe.boekelheide@nist.gov

[1] Z. Boekelheide, A. X. Gray, C. Papp, B. Balke, D. A. Stewart, S. Ueda, K. Kobayashi, F. Hellman, and C. S. Fadley, Phys. Rev. Lett. **105**, 236404 (2010).

[2] D. J. Chakrabarti and P. A. Beck, J. Phys. Chem. Solids **32**, 1609 (1971).

[3] L. V. Nomerovannaya and V. A. Rassokhin, Phys. Status Solidi A **79**, 87 (1983).

[4] N. Pessall, K. P. Gupta, C. H. Cheng, and P. A. Beck, J. Phys. Chem. Solids **25**, 993 (1964).

[5] E. Fawcett, H. L. Alberts, V. Y. Galkin, D. R. Noakes, and J. V. Yakhmi, Rev. Mod. Phys. **66**, 25 (1994).

[6] W. Koster, E. Wachtel, and K. Grube, Z. Metallkd. **54**, 393 (1963).

[7] A. Kallel and F. deBergevin, Solid State Commun. **5**, 955 (1967).

[8] E. Fawcett, Rev. Mod. Phys. **60**, 209 (1988).

[9] M. M. R. Costa and P. J. Brown, J. Phys. F **7**, 493 (1977).

[10] F. J. A. den Broeder, G. van Tendeloo, S. Amelinckx, J. Hornstra, R. de Ridder, J. van Landuyt, and H. J. van Daal, Phys. Status Solidi A **67**, 233 (1981).

[11] J. L. Murray, J. Phase Equilib. **19**, 367 (1998).

[12] Z. Boekelehide, D. A. Stewart, and F. Hellman, Phys. Rev. B (submitted, 2012).

[13] E. E. Fullerton, M. J. Conover, J. E. Mattson, C. H. Sowers, and S. D. Bader, Phys. Rev. B **48**, 15755 (1993).

[14] L. J. van der Pauw, Philips Tech. Rev. **20**, 220 (1958).

[15] S. A. Danilkin, G. Horton, R. Moore, G. Braoudakis, and M. E. Hagen, J. Neutron Res. **15**, 55 (2007).

[16] E. E. Fullerton, S. D. Bader, and J. L. Robertson, Phys. Rev. Lett. **77**, 1382 (1996).

[17] *Neutron Data Booklet*, edited by A.-J. Dianoux and G. Lander (OCP Science, Philadelphia, 2003).

[18] V. F. Sears and S. A. Shelley, Acta Crystallogr. Sect. A **47**, 441 (1991).

[19] M. Birkholz, *Thin Film Analysis by X-Ray Scattering* (Wiley-VCH, Weinheim, 2006).

[20] Density-functional theory calculations give an Al moment less than $0.03\mu_B$.

[21] The Al peak shifts significantly toward the Cr_3Al peak at higher temperatures due to the large thermal expansion of Al. In addition, the Cr_3Al (002) peak is at a higher q in the 600°C sample than the 300°C sample due to the previously discussed tetragonal distortion.

[22] M. Atoji, J. Chem. Phys. **43**, 222 (1965).

[23] [http://sham.phys.sci.osaka-u.ac.jp/kkr/].

[24] J. Korringa, Physica **13**, 392 (1947).

[25] W. Kohn and N. Rostoker, Phys. Rev. **94**, 1111 (1954).

[26] J. P. Perdew, J. A. Chevary, S. H. Vosko, K. A. Jackson, M. R. Pederson, D. J. Singh, and C. Fiolhais, Phys. Rev. B **46**, 6671 (1992).

[27] P. Soven, Phys. Rev. **156**, 809 (1967).

[28] H. Akai, J. Phys. Condens. Matter **1**, 8045 (1989).

[29] R. Hafner, D. Spišák, R. Lorenz, and J. Hafner, Phys. Rev. B **65**, 184432 (2002).

[30] J. Li, H. Chen, Y. Li, Y. Xiao, and Z. Li, J. Appl. Phys. **105**, 083717 (2009).

[31] M. A. Lind and J. L. Stanford, J. Phys. Soc. Jpn. **53**, 4029 (1984).

[32] R. M. Martin, *Electronic Structure: Basic Theory and Practical Methods* (Cambridge University Press, Cambridge, 2005).

[33] H. Akai and J. Kanamori, J. Phys. Soc. Jpn. **54**, 3537 (1985).

[34] S. Roth and J. Sonntag, Phys. Status Solidi B **87**, K69 (1978).